Structures 52 (2023) 1087–1100

Contents lists available at ScienceDirect

Structures

journal homepage: www.elsevier.com/locate/structures

Impact of rail joints on the local stresses in crane runway girders

Markus Kettler *, Thomas Jurschitsch, Harald Unterweger

Institute of Steel Structures, Graz University of Technology, Austria

ARTICLE INFO

Keyword:
Crane runway girder
Wheel loading
Local stresses
Rail joint

ABSTRACT

Vertically acting wheel loads from overhead bridge cranes and potential additional horizontal crane loads induce global stresses due to bi-axial bending and torsion and local stresses in crane runway girders which mainly affect the girder's web. The latter typically represent one of the most decisive criteria for the fatigue design check of welded girders and are the focus of this paper. Crane rails with foot flange are typically used for moderate to high wheel loads. They are usually connected to the top flange with rail clips. Rails with foot flange are used with and without elastomeric bearing pads between the rail and the top flange of the girder. The local stresses in the webs of crane runway girders are strongly affected by discontinuities of the crane rails. Such discontinuities can originate from unplanned rail cracks as well as planned rail expansion joints. The current mechanical models for concentric as well as eccentric wheel loading in relevant design standards assume continuous crane rails. However, rail joints are expected to significantly increase the local stresses in the region beneath rail joints. The present paper focuses on the impact of rail joints on the local stresses in crane runway girders. The research activities comprise experimental tests as well as numerical parametric studies based on finite element calculations, both for rails with and without elastomeric bearing pads. The aim of the investigations is to develop a better understanding of the mechanical behaviour and to quantify the increase factor for maximum local stresses in order to avoid future fatigue damage due to an unexpected increase of local stresses at a rail joint.

1. Introduction

1.1. General

Overhead bridge cranes are used to carry heavy loadings within industrial buildings. Thereby, they usually travel along crane runway girders. The wheel loads from these cranes generally include dynamic effects and they are transferred to the crane runway girder through crane rails which are located at the top of the girder. The recurring nature of these actions require verification of fatigue resistance of the steel girder. Vertically acting wheel loads and potential additional horizontal crane loads induce two types of stresses in the crane runway girder: i) global stresses due to bi-axial bending and torsion and ii) local stresses, with dominating vertical normal stresses, which mainly affect the girder's web. Both types of stresses have to be considered (and superposed where necessary) for design purposes. It is assumed that the horizontal crane loads occur randomly scattered along the crane runway girder. Therefore, they are considered for ultimate and serviceability limit states, but they are generally not considered for fatigue verifications. The local stresses near the connection between the web and the top flange (resulting from wheel loads) typically represent one of the most decisive criteria for the fatigue design check of welded girders. In addition, one travel of the crane leads to several local stress ranges, depending on the number of crane wheels. This further increases the importance of this detail for a safe and economic design.

1.2. Concentric wheel loading

Several researchers investigated the local stresses in crane runway girders resulting from wheel loads and their influence on the fatigue life in the past. The first investigations focused on the membrane stresses in the web due to concentric wheel loads (i.e. wheel loads that act in the plane of the web), [1–4]. In [1] Girkmann presented a closed solution for the maximum vertical compression stresses in the web directly under a single wheel load. The utilized model consists of a beam (i.e. the top flange plus the crane rail) with infinite length situated at the top edge of a web plate with infinite length and depth. No shear is transferred between beam and plate. In [2] Parkes derived the vertical compression stresses along the top edge of the web for two cases. First, flange resting on a semi-infinite plane. Second, beam of finite depth. He showed that

* Corresponding author at: Institute of Steel Structures, Graz University of Technology, Lessingstraße 25/III, 8010 Graz, Austria.
E-mail address: kettler@tugraz.at (M. Kettler).

https://doi.org/10.1016/j.istruc.2023.04.046
Received 1 February 2023; Received in revised form 12 April 2023; Accepted 12 April 2023
Available online 21 April 2023

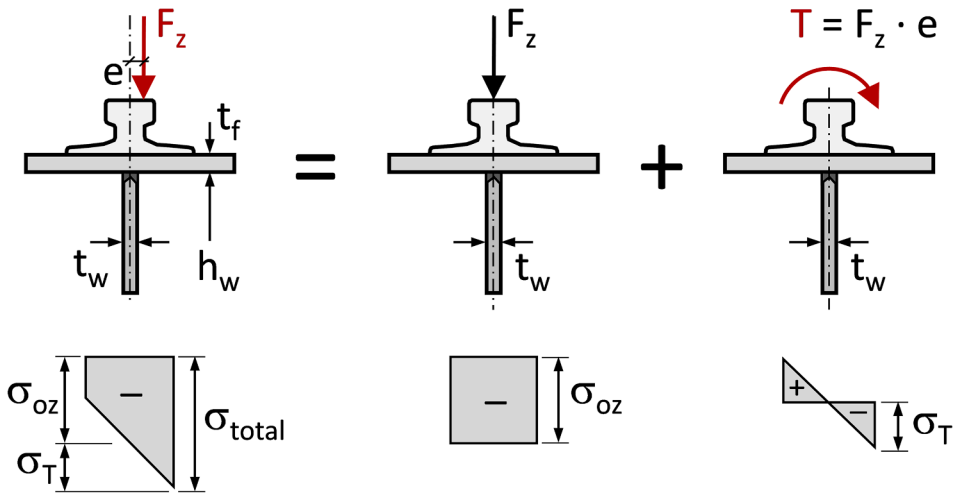

Fig. 1. Local stresses at the web top due to eccentric vertical wheel load F_z.

for most practical cases, the first solution (which is basically the same solution as in [1]) gives sufficient accurate results. In addition, three experimental test results were presented with focus on the global direct stresses. No measurements of vertical stresses were performed. In [3] Rieve gave a set of equations for the calculation of the complete plane stress field at any position of the web plate with finite height. The maximum vertical compression stresses at the top edge of the web approximately correspond to those of the two before mentioned publications. Moreover, three experimental tests on IP 32 sections (which approximately correspond to the European hot rolled section HEB 320) were presented. However, only one test specimen was equipped with strain gauges (five on each side of the web) to measure the local vertical strains. In [4] Vögele presented a complete set of formulae for calculating the global and local direct stresses and the corresponding shear stresses in the web plate of a girder with finite height. This was realized by considering the actual axial stiffness of the flanges. The author additionally gave a comparison with a test result from literature that showed good agreement (differences <10%).

1.3. Eccentric wheel loading

Generally, the vertical wheel load F_z will show a certain eccentricity e compared to the mid-surface of the web plate. This will lead to local vertical transverse bending stresses σ_T in the web in addition to the already discussed local membrane stresses σ_{oz} from concentric wheel load, as shown in Fig. 1. Note that the additional bending stresses σ_T may be neglected for low fatigue exposure according to EN 1993–6.

The maximum bending stresses are located near the web-flange connection, directly beneath the wheel load. In [5,6] Oxfort presented the theoretical background of a simplified model for the calculation of the maximum bending stresses due to eccentric wheel loading. The engineering model consists of a beam (representing the rail and the top flange of an I-shaped girder) of length a between two transverse stiffeners of the crane runway girder. It is assumed that the transverse stiffeners provide fork end conditions for this beam. The external moment $T = F_z \cdot e$ is acting at mid-length between the two supports, where it results in the maximum local bending stresses in the web. The torsional stiffness GI_t of the idealised beam generally consists of the sum of the torsional stiffness of the upper flange of the girder and the crane rail. The contribution of the web plate is considered by means of an elastic torsional restraint for the beam. By assuming this torsional restraint to be constant over the member length between two adjacent transverse stiffeners, the differential equation for the rotation of the member can be solved. In all mentioned investigations no elastomeric bearing pad between rail and top flange of the girder was considered. In [7] the authors enhanced this model and extended the scope of application also for crane runway girders with box section. The enhanced model allows for consideration of the additional stiffness contribution of the upper flange. The analytical results were compared with test results and additional numerical finite element calculations of crane runway girders with welded box sections. It was shown that the derived formula for box sections produces results that have the same quality of accordance as the corresponding results for I-sections. It was also verified that additional longitudinal web stiffeners increase the transverse bending stresses in the web plate due to eccentric wheel loading. Therefore, the authors subsequently investigated the influence of longitudinal stiffeners on the local stresses systematically, [8,9]. It was shown that the position of the longitudinal stiffener significantly affects the local transverse bending stresses. A proposal for the consideration of additional stiffeners was given. The comparison with experimental and numerical results for I-shaped girders indicated that this proposal can appropriately describe the additional web-stiffening effect.

1.4. Rail-to-flange connection types

For practical applications, basically two different types of crane rails are used: i) flat rails for smaller wheel loads and ii) crane rails with foot flange for intermediate to large wheel loads. Flat rails are generally welded to the top flange by means of continuous or intermittent rail welds. Crane rails with foot flange are typically connected to the top flange with rail clips. These clips maintain the position of the rail in vertical and horizontal transverse direction, but they generally allow for longitudinal movement of the rail. Rails with foot flange are used with and without elastomeric bearing pads between the rail and the top flange of the girder. The influence of various rail types as well as different types of connection and contact on the local stresses were subject of several research activities in the past. In [10] Steinhardt and Schulz derived a procedure for calculating the local stresses in the web due to concentric wheel loading for cases with elastomeric bearing pad. In addition, experimental tests with and without elastomeric bearing pad and with concentric wheel loading were carried out. It was concluded that usage of such a pad reduces the corresponding local stresses by 20–40%. Further theoretical investigations on the impact of elastomeric bearing pads were carried out by Hoffmann and can be found in [11–13]. In [14] the authors reported on tests on a hot rolled HEA 300 girder. Results are presented for wheel load introduction, i) directly on the top flange of the girder without rail, ii) on girder with flat rail without welded connection to the top flange and iii) the practical case of the flat rail being welded continuously to the top flange. The influence of elastomeric bearing pads on the local stresses in the web and

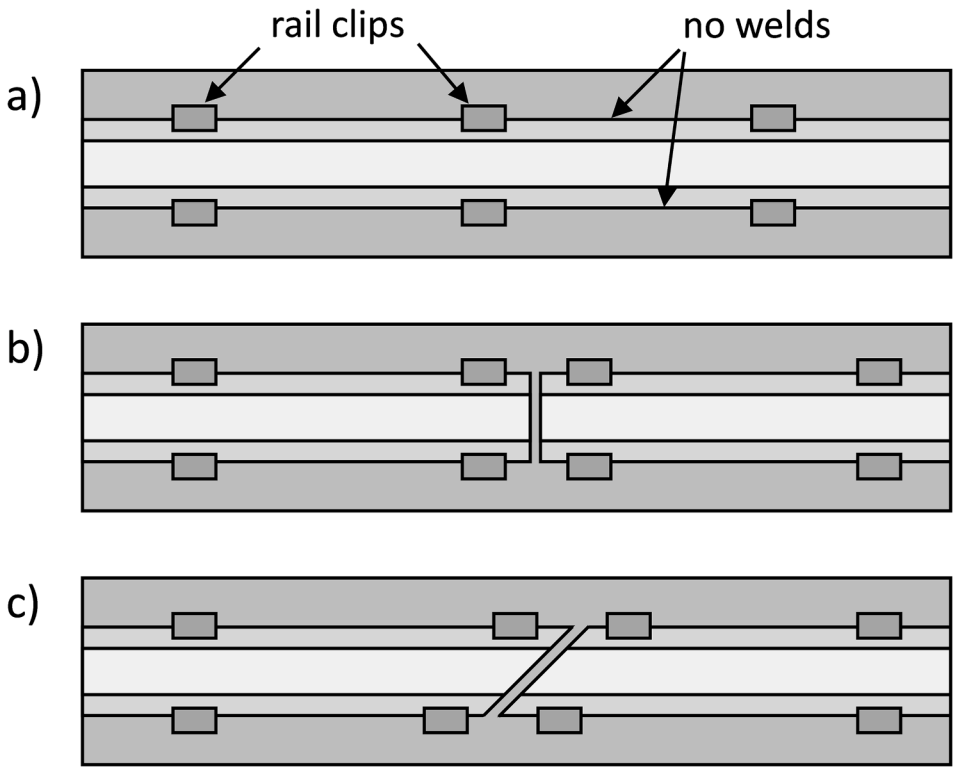

Fig. 2. Top view on crane rails with foot flange on girder: a) continuous rail, b) orthogonal joint, c) bevel joint.

in the crane rail was investigated by the authors in [8,9,15]. Another test on a retrofitted crane runway girder with boxed upper flange can be found in [16]. Furthermore, a design concept for the calculation of local bending stresses in webs of retrofitted crane runway girders was proposed, for both types of strengthening (box or triangular section of upper flange).

1.5. Fatigue strength of details loaded by wheel loads

The so far discussed research activities focused on the understanding of the loading side of the verification procedure for the fatigue resistance of crane runway girders made of steel. In conclusion of this introduction, also test-based research output on the fatigue strength of specific details loaded by wheel loads is summarized shortly. In [17–19] fatigue tests on welded girders with flat rails were presented with pulsating stationary wheel load and with travelling wheel load. The investigated welds at the connections between flange and web of the girder and between flange and flat rail were fillet welds. In [7,20,21] fatigue tests on crane runway girders (or part of girders) with full penetration welds between the web and flange of the girder were carried out. In [22] in situ strain measurements were conducted on welded crane runway girders with full penetration welds during operation of the bridge cranes. Based on these results, recommendations for the fatigue classification of full penetration welds were given. The positive effect of high frequency mechanical impact treatment (i.e. post-weld treatment) on the fatigue strength of welded details in crane runway girders was illustrated in [23]. It was shown that this procedure can also be applied on existing structures if certain restrictions are considered. In [24] typical mistakes in planning, manufacturing and operation of crane girders are summarized and recommendations of how to avoid them are given.

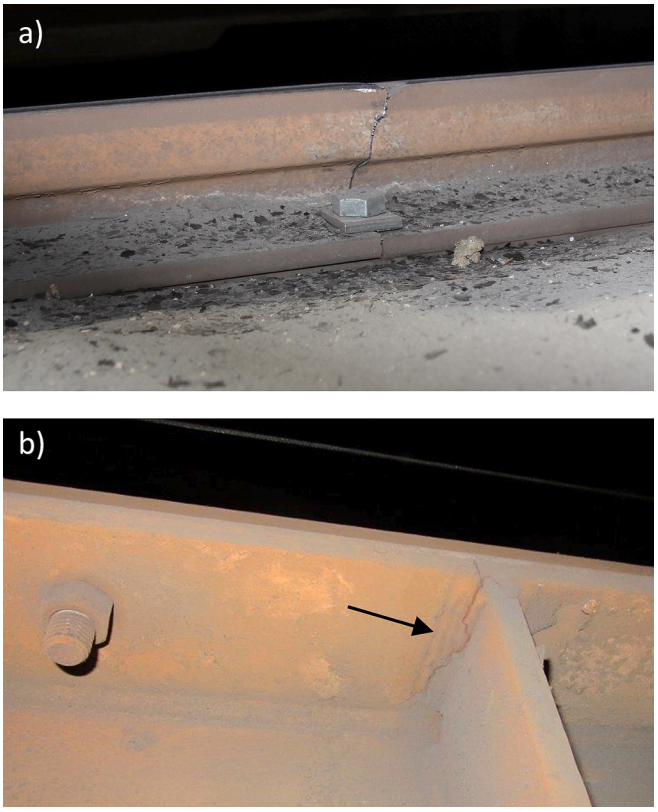

Fig. 3. a) Through-thickness crack of crane rail, b) cracks in fillet welds of transverse stiffener at the connection to the top flange of the girder.

1.6. Effect of rail joints

Rails with foot flange can be installed as continuous rails with welded splices or they can be discontinuous with expansion joints at certain

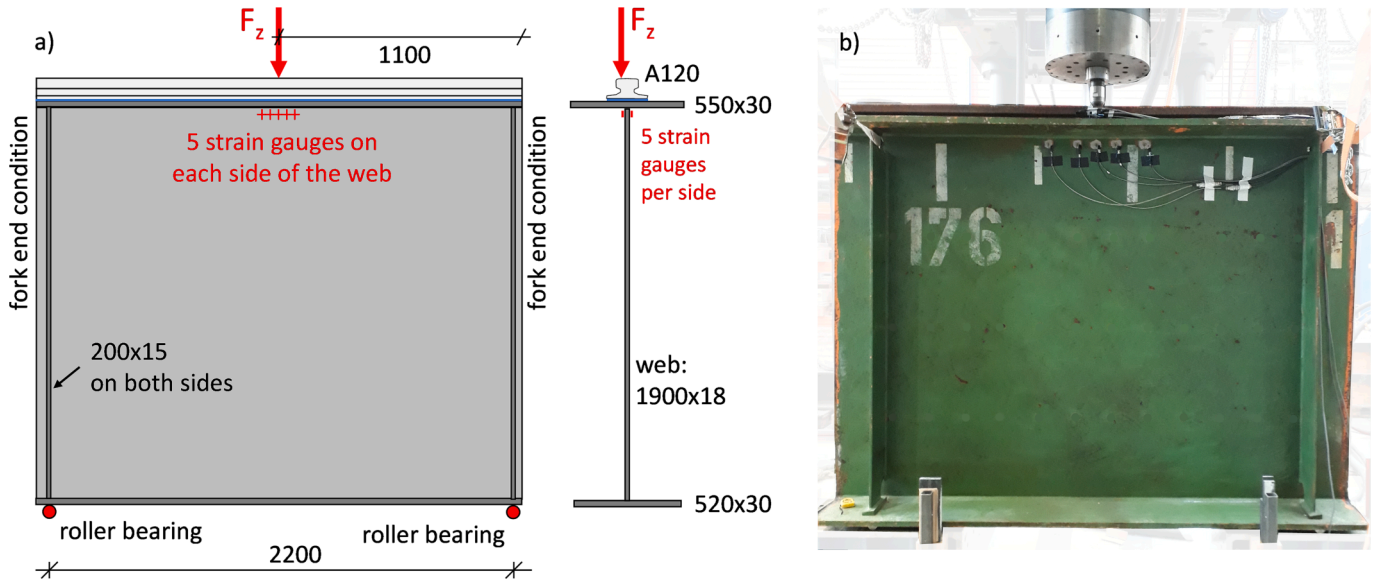

Fig. 4. a) Geometry, support conditions and load introduction for the test girder, b) test girder in testing machine (all dimensions in mm).

locations. Expansion joints are typically realized with bevel joints, but they can also be realized with orthogonal joints, see Fig. 2.

Bevel joints are used to improve smoothness of operation compared to orthogonal joints. However, this comes with the disadvantage of higher wear and tear. To improve the smoothness of operation even further, stepped bevel joints are used in some rare cases. Their application is limited, because of higher expenses for production. Continuous rails with modern elastomeric bearing pads and rail clips also allow for relative longitudinal movement. Therefore, expansion joints seem not to be necessary for new installations. However, they are still used in practice.

The local stresses in the webs of crane runway girders are strongly affected by discontinuities of the crane rails. The mechanical models for concentric as well as eccentric wheel loading assume continuous crane rails. Rail joints are therefore expected to significantly increase the local stresses in the region beneath the expansion joints. This fact was also illustrated in [25] based on four finite element calculations (one with continuous rail and three with different types of expansion joints).

Discontinuities in crane rails can also originate from unplanned rail cracks, see Fig. 3a. The illustrated crack in the rail of type A120 initiated at the bolted connection of the foot flange and led to a complete through-thickness crack. As a result of this damage, the local stresses in the region beneath the unplanned rail discontinuity significantly increased, which favoured the initiation of further cracks in the top fillet welds of a nearby transverse stiffener – probably in connection with longitudinal normal stresses in the top flange, see Fig. 3b.

The present paper investigates the impact of rail joints on the local stresses in crane runway girders. The focus is on the elastic stress field, which is relevant for fatigue design. Local plasticity effects are not considered, because rail joints generally don't have relevant influence on the ultimate capacity of crane runway girders. For most practical cases, the dimensions of the girder are defined by fatigue verifications. However, the increased local stresses below rail joints are still significantly lower than the yield strength. The research activities comprise experimental tests as well as numerical parametric studies based on finite element calculations. The aim of the investigations is to develop a better understanding of the mechanical behaviour in order to avoid future fatigue damage due to an unexpected increase of local stresses at a rail joint.

2. Analytical formulae for local stresses

In the following, analytic formulae for the calculation of the maximum vertical local stresses in webs of crane runway girders are summarized (σ_{total} in Fig. 1). They are used for comparison of the test and numerical results. Eqs. (1)–(4) are presented in the format of EN 1993-6, [26]. Eqs. (1) and (2) allow for calculating the maximum local vertical stresses at the upper edge of the web due to concentric wheel loading.

$$\sigma_{oz} = \frac{F_z}{l_{eff} \cdot t_w} \tag{1}$$

Where F_z is the vertical wheel load, t_w is the thickness of the web and l_{eff} is an effective length depending on the rail to flange connection. For cases with rails welded to the top flange (typically flat rails), Eq. (2a) should be used to calculate the effective length. I_{rf} is the moment of inertia about the horizontal axis of the combined cross-section comprising the rail and the top flange.

$$l_{eff} = 3.25 \left(\frac{I_{rf}}{t_w} \right)^{1/3} \tag{2a}$$

For cases where the rail is not rigidly fixed to the top flange and no elastomeric bearing pad is installed, Eq. (2b) should be used. I_r is the moment of inertia of the rail and $I_{f,eff}$ is the moment of inertia of the top flange with an effective width $b_{eff} = t_f + b_{fr} + h_r$, where t_f is the thickness of the flange, b_{fr} is the width of the rail foot and h_r is the height of the rail.

$$l_{eff} = 3.25 \left(\frac{I_r + I_{f,eff}}{t_w} \right)^{1/3} \tag{2b}$$

For cases with additional elastomeric bearing pad under the crane rail, Eq. (2c) should be used.

$$l_{eff} = 4.25 \left(\frac{I_r + I_{f,eff}}{t_w} \right)^{1/3} \tag{2c}$$

Eqs. (3) and (4) allow for calculating the local transverse bending stresses in the web due to eccentric wheel loading, ignoring the effect of additional elastomeric bearing pads.

$$\sigma_T = \frac{6 \cdot T}{a \cdot t_w^2} \cdot \eta \cdot tanh(\eta) \tag{3}$$

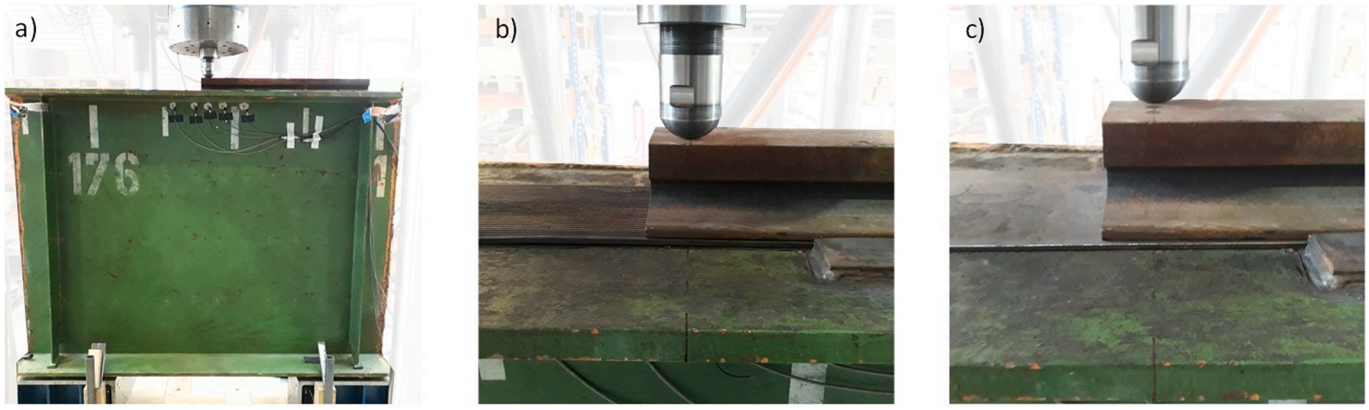

Fig. 5. a) Test girder and rail with orthogonal joint in testing machine, b) rail with orthogonal joint on elastomeric bearing pad, c) rail with orthogonal joint on steel bearing plate.

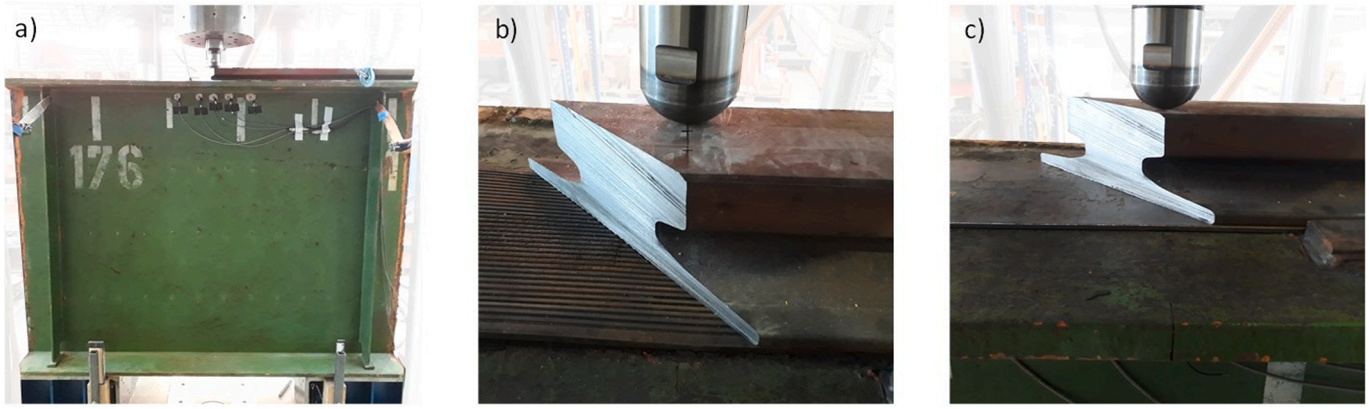

Fig. 6. a) Test girder and rail with bevel joint in testing machine, b) rail with bevel joint on elastomeric bearing pad, c) rail with bevel joint on steel bearing plate.

$$\eta = \left[\frac{0.75 \cdot a \cdot t_w^3}{I_t} \cdot \frac{sinh^2\left(\frac{\pi \cdot h_w}{a}\right)}{sinh\left(\frac{2\pi \cdot h_w}{a}\right) - \frac{2\pi \cdot h_w}{a}} \right]^{0,5} \tag{4}$$

Where $T = F_z \cdot e$, a is the spacing of transverse stiffeners, h_w is the depth of the web and I_t is the sum of the torsional constants of the top flange and the rail (including the contribution of the composite action only if the rail is rigidly fixed).

For design purposes, the total stress σ_{total} due to the eccentric wheel load F_z can be calculated by means of Eq. (5).

$$\sigma_{total} = \sigma_{oz} + \sigma_T \tag{5}$$

3. Experimental tests

Several experimental tests were carried out on an old crane runway girder that has been replaced by a new girder during renovation of the surrounding steel hall. The investigated girder has the following dimensions: top flange 550 × 30 mm, bottom flange 520 × 30 mm, web plate 1900 × 18 mm and a crane rail of type A120 that was originally supported by a resilient elastomeric bearing pad of 6 mm thickness. In the laboratory, tests with and without elastomeric bearing pad were conducted. For cases without elastomeric bearing pad, a steel bearing plate of 6 mm thickness was used instead. Transverse stiffeners were located at distances of 2200 mm. The test girder is a single span beam that consists of a part of the original girder with two transverse stiffeners at the ends that served as stiffeners at the supports in the laboratory tests, see Fig. 4. The material of the girder is a steel S235 with a nominal yield strength of $f_y = 235$ N/mm^2. Based on the fact that the maximum stresses are significantly below the yield stress, no additional tension tests were conducted. Note: The same test girder was used in [9] for the investigation of the influence of longitudinal stiffeners on the local stresses in the web.

Ten strain gauges (5 on each side of the web) were used to measure the local vertical strains in the web plate near the load introduction at mid-span. The measurement devices were applied 40 mm below the top edge of the web plate. This distance was chosen to minimize the influence of the welded connection (full penetration weld) between web and top flange on the measurement results. The individual strain gauges had a distance in longitudinal direction from the load introduction of 0 mm, 100 mm or 250 mm, thus a total length of 500 mm was considered. The vertical load F_z was applied displacement-controlled and it was increased until a maximum strain of approximately 1.1‰ was measured in the strain gauges. This procedure should ensure pure elastic behaviour of the investigated web plate region. After testing, the measured strains decreased to zero again, also confirming elastic behaviour. The load introduction was realized via a piston with spherical head that only allowed for vertical movement, see Figs. 4–6. Concentric tests with $e = 0$ as well as eccentric tests with $e = \pm 30$ mm were carried out. The different eccentricities (perpendicular to the longitudinal axis of the crane rail) were realised by adapting the position of the test girder in relation to the testing rig. Roller bearings were situated directly under the transverse stiffeners at the ends of the girder.

In total 18 elastic tests were carried out: i) 6 tests for cases with continuous rails (Fig. 4b), ii) 6 tests with orthogonal rail joints (Fig. 5) and iii) 6 tests with bevel rail joints (Fig. 6). For each of the three rail configurations, the 6 tests were divided into tests with three different

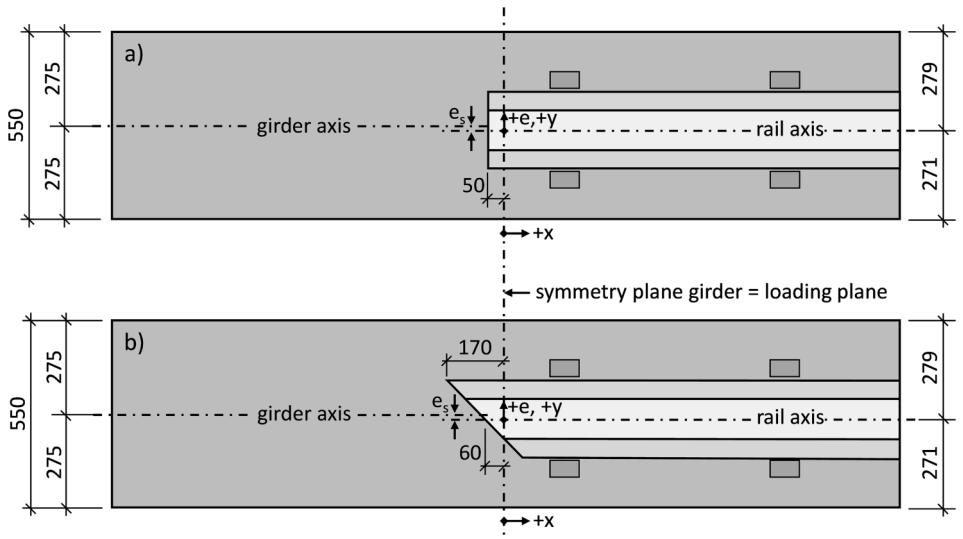

Fig. 7. Top views of test girder and position of load introduction: a) orthogonal rail joint, b) bevel rail joint. (Note: based on the orientation of the load eccentricity, the eccentricity of the rail is $e_s = -4$ mm; all dimensions in mm).

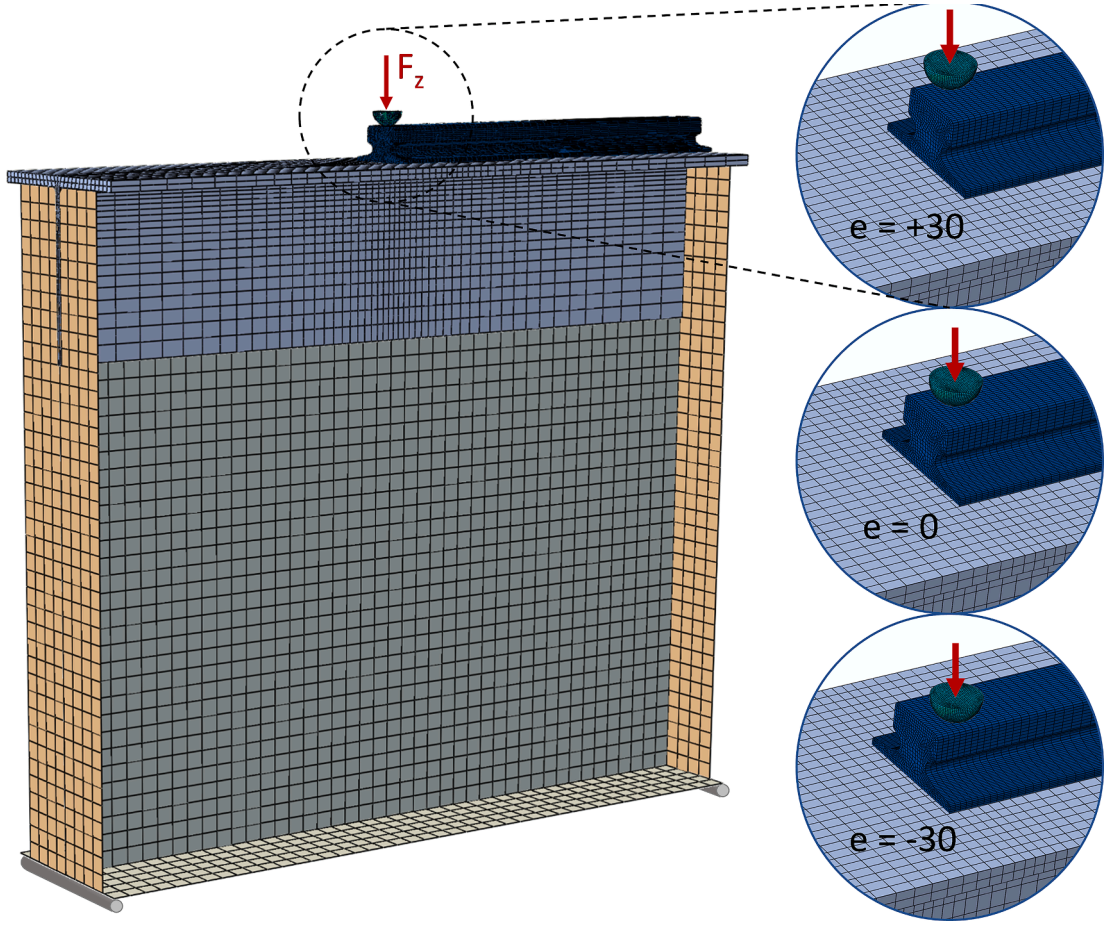

Fig. 8. FE model of test girder with orthogonal rail joint and load introduction at positions $e = 0$ and $e = \pm 30$ mm.

eccentricities ($e = 0, \pm 30$ mm) with the original elastomeric bearing pad (Fig. 5b and 6b) and with a steel bearing plate (Fig. 5c and 6c), respectively. All rail heads showed relatively small abrasion of approximately $\Delta h_r = 2$ mm. For the tests with rail joints only the loaded rail was part of the test configuration, due to the fact that for the practical cases in Fig. 2 the unloaded rail part gets no stresses at all.

Fig. 7 presents two top views of the test girder including the geometry of the rails with orthogonal joint and bevel joint, respectively.

The position of the loaded part of the rail was 4 mm eccentric to the mid-plane of the girder's web ($e_s = -4$ mm). This was enforced by a lateral guiding system that was originally welded to the top of the girder's top flange. The corresponding steel blocks can be seen in Fig. 5b,

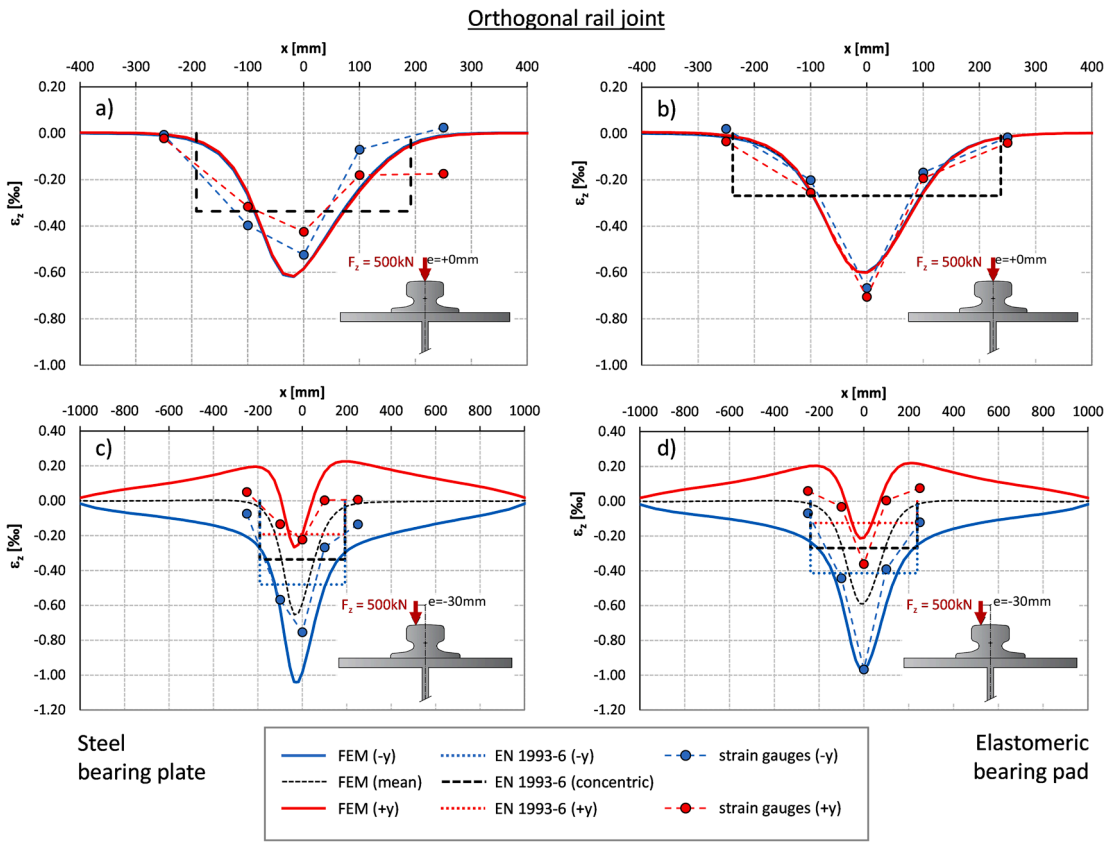

Fig. 9. Comparison of results for test girder with orthogonal rail joint and $F_z = 500$ kN: a) steel bearing plate and $e = 0$, b) elastomeric bearing pad and $e = 0$, c) steel bearing plate and $e = -30$ mm, d) elastomeric bearing pad and $e = -30$ mm.

c and 6c. The rail clips were not installed for testing, but the eccentric position of the rail with $e_s = -4$ mm was retained. The loading plane corresponds to the symmetry plane of the test girder and is also illustrated in Fig. 7. The key results of the physical tests are presented in section 4.2 together with the results of additional finite element calculations of the test girder.

4. Numerical simulations and comparison with test results

4.1. Finite element model

In addition to the laboratory tests, finite element calculations of all test configurations were carried out with the software Abaqus. The crane rail was modelled with linear brick elements (C3D8R), the top flange and the upper quarter of the web were modelled with quadratic brick elements (C3D20R, two elements over the thickness of the plates). The rest of the girder was modelled with linear shell elements (S4R). Fig. 8 shows an overview of this optimized FE-model with these specific element types and element sizes. The basis of this FE-model was developed in [9] based on comprehensive sensitivity studies to guarantee accurate stress values near the top of the girder's web. To reduce computing time, the lower part of the web, the lower flange and the vertical stiffeners have a course meshing. It was ensured that this fact has no negative influence on the quality of the investigated local stresses in the upper part of the web near the load introduction.

The material was linear elastic with a Young's modulus $E = 210{,}000$ N/mm^2 and a Poisson ratio of $\nu = 0.3$. The elastomeric bearing pad and the steel bearing plate, respectively, were modelled by means of specific contact interactions. The elastomeric bearing pad had a normal stiffness of 20 N/mm^3 (i.e. a distributed load of 20 N/mm^2 leads to an overall vertical deformation of 1 mm), while the steel bearing plate was assumed as incompressible. The latter was considered via hard contact conditions between rail and top flange (i.e. the steel plate was not explicitly modelled.). Therefore, the case with steel bearing plate is identical to cases without any load distributing elements between the rail and the top flange. Separation of the contact surfaces was possible. In tangential direction, the friction coefficient was set to 0.1, but this had no significant influence on the investigated local stresses in the web. The actual position of the crane rail ($e_s = -4$ mm) as well as the actual wear of the rail head ($\Delta h_r = 2$ mm) were considered corresponding to the measurements in the laboratory. The welded connection between the top flange and the web plate was realised through a double bevel butt weld with additional fillet welds $a = 9$ mm. This was considered in the numerical model by assuming full contact between the top flange and the web. The geometry of the additional fillet welds was modelled by means of a pair of isosceles triangles and meshed with quadratic brick elements. The loading was introduced via a hemisphere with radius $r = 40$ mm, which corresponded to the head of the loading piston of the experimental tests. Fig. 8 exemplarily shows the finite element model of the test girder with orthogonal rail joint and the load introduction at the three investigated load positions $e = 0$ and $e = \pm 30$ mm. The roller bearings under the vertical stiffeners at the supports were modelled by restraining the vertical and transversal deformations at the ends of the lower flange.

4.2. Comparison with test results

In the following, the results of the numerical calculations are compared with the test results and with code predictions. The latter are based on Eqs. (1), (2b) and (2c) for concentric loading and on Eqs. (3) and (4) for the additional bending part due to eccentric wheel loading. The comparison is made on the basis of vertical strains in the web plate at a distance of 40 mm from the top flange. The calculated vertical stresses σ_z from Eqs. (1) and (3) (based on the simplified analytical

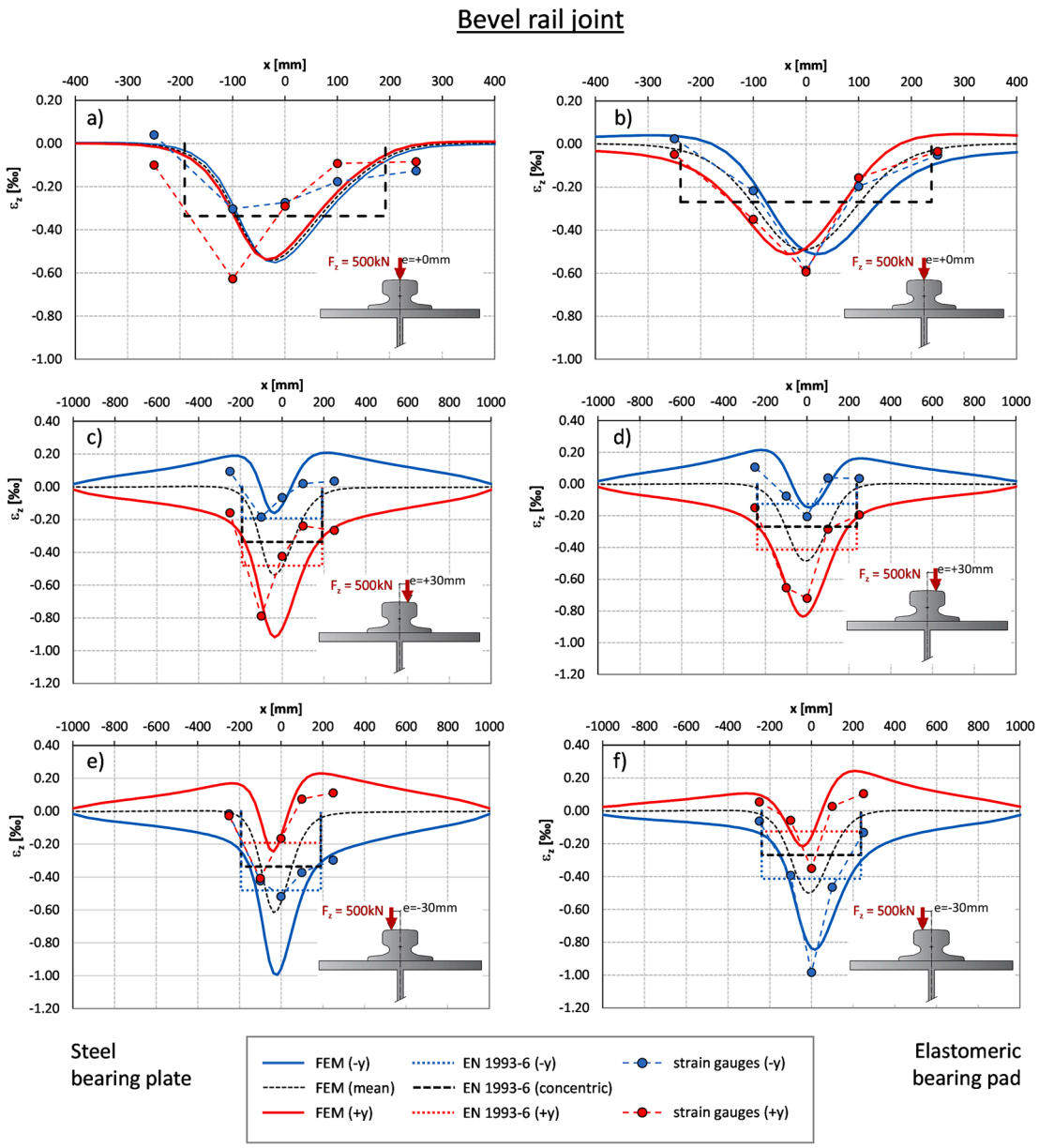

Fig. 10. Comparison of results for test girder with bevel rail joint and $F_z = 500$ kN: a) steel bearing plate and $e = 0$, b) elastomeric bearing pad and $e = 0$, c) steel bearing plate and $e = +30$ mm, d) elastomeric bearing pad and $e = +30$ mm, e) steel bearing plate and $e = -30$ mm, f) elastomeric bearing pad and $e = -30$ mm.

model in EN 1993–6) are converted to vertical strains ε_z under the consideration of a simplified plane stress state in the girder's web, see Eq. (6).

$$\varepsilon_z = \frac{1}{E}\cdot(\sigma_z - \nu\cdot\sigma_x) \tag{6}$$

The longitudinal stresses σ_x were calculated based on beam theory, although Bernoulli hypothesis is not fully accurate for the very short span of the girder. Nevertheless, due to the short span of the test girder, the influence of longitudinal stresses on the vertical strains was generally rather small (smaller than 3% difference compared to the case with $\sigma_x = 0$). Considering the actual stresses σ_x and τ from the finite element results does not significantly change the converted strains ε_z.

Fig. 9 presents a comparison of results for the test girder with orthogonal rail joint and a wheel load of $F_z = 500$ kN. Fig. 9a and b show the results for concentric wheel loading and Fig. 9c and d show the results for eccentric wheel loading ($e = -30$ mm). Note: The results for $e = +30$ mm show very similar results and are therefore not included in Fig. 9 (different results expected due to the measured eccentricity $e_s = -4$ mm of the crane rail). The vertical strains based on the FE-calculations are plotted on the inner and outer web surface (FEM (−y) and (+y)) and in the web axis (FEM (mean)). For the definition of the positive e- and y-direction see Fig. 7. Fig. 9a and c illustrate the cases with steel bearing plate under the rail while Fig. 9b and d cover the cases with elastomeric bearing pad.

The comparison of finite element results (FEM) with the measurements (strain gauges) shows reasonable agreement. Larger differences of up to 25 % are found for the case of steel bearing plate under the crane rail (Fig. 9a,c). The reason for these discrepancies is the unevenness in the interface between the top flange (upper surface) and the crane rail (lower surface). The significant influence of the contact conditions was also found in recently conducted similar experimental tests by the authors [9]. Fig. 9 indicates that the elastomeric bearing pad is able to compensate this effect to a certain degree. The comparison for cases with elastomeric bearing pad shows good agreement (Fig. 9b,d). Based on the comparison in Fig. 9, it is concluded that the numerical model is able to

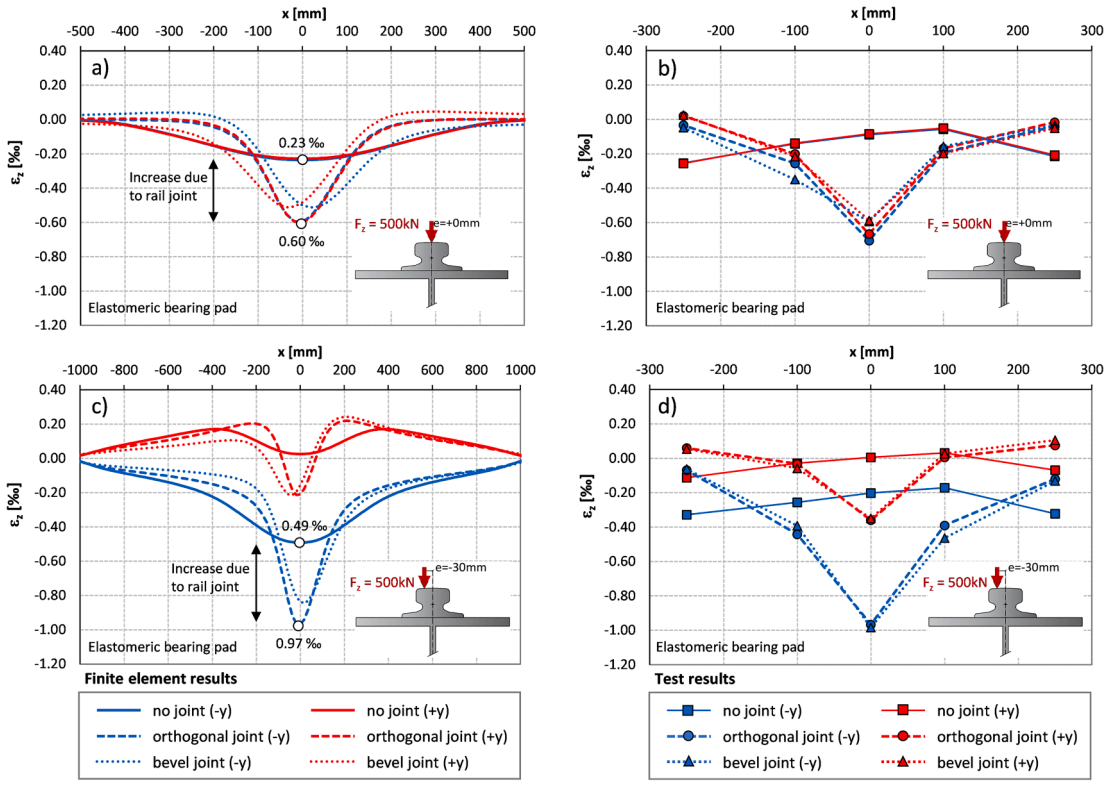

Fig. 11. Comparison of results for test girder with and without rail joints, elastomeric bearing pad and $F_z = 500$ kN: a) FEM results and $e = 0$, b) test results and $e = 0$, c) FEM results and $e = -30$ mm, d) test results and $e = -30$ mm.

describe the real behaviour sufficiently accurate. The numerical results for concentric loading reveal that the influence of the rail eccentricity e_s (see Fig. 7) is negligible. By comparing the numerical results with elastomeric bearing pad and with steel bearing plate, it is found that the maximum vertical strains are approximately of the same size for both cases. This fact is found for concentric as well as eccentric loading. The typical beneficial effect of elastomeric bearing pad under the rail is lost due to the orthogonal rail joint. The code predictions (EN 1993-6) do not consider any rail joint and these resulting vertical strains are therefore significantly smaller than the strains from test and FEM.

Fig. 10 shows a comparison of results for the test girder with bevel rail joint. The wheel load is again $F_z = 500$ kN. Fig. 10a, c and e present the cases with steel bearing plate. Fig. 10b, d and f illustrate the cases with elastomeric bearing pad. Results for concentric and eccentric loading ($e = \pm 30$ mm) are given. By comparing the finite element results (FEM) with the measurements (strain gauges), the quality of the numerical model with bevel joint in the crane rail can be confirmed. In particular, the cases with elastomeric bearing pad under the rail show very good agreement. The measurements with steel bearing plate under the rail with bevel joint are apparently very sensitive to local contact conditions between rail, steel plate and top flange. This can best be verified by the example of Fig. 10a and e. For the concentric loading case in Fig. 10a, the measured vertical strains are significantly smaller on the (−y) surface of the web (blue dashed curve) than the measured strains on the (+y) surface (red dashed curve) and also the maximum values are shifted in longitudinal direction (to x = −100 mm). It is assumed that this effect originates from varying contact conditions under the crane rail. The hard steel bearing plate is not able to distribute the acting stresses smoothly over the whole contact area as it is the case for the elastomeric bearing pad. Even for the case of eccentric wheel loading with $e = -30$ mm, the measured strains in Fig. 10e on the (−y) surface of the web are only marginally larger than the corresponding strains on the (+y) surface for x < 100. In contrast to that, the measured strains with elastomeric bearing pad in Fig. 10f on the (−y) surface are over the whole length larger than the (+y) surface strains by more than a factor of 2.5. The comparison of maximum compression strains of the finite element calculations with and without elastomeric bearing pad reveals that for bevel rail joints with elastomeric bearing pad the strains are slightly smaller than for cases with steel bearing plate. The predicted maximum strains according to EN 1993–6 are significantly smaller than the strains from test and FEM.

Fig. 11 presents a comparison of results of finite element calculations and test measurements with rail joints with the reference case of continuous crane rails without joint. Finite element results are shown in Fig. 11a and c, test measurements are presented in Fig. 11b and d. The test girder is loaded by $F_z = 500$ kN for all cases. An elastomeric bearing pad is situated under the crane rail. Results are shown for concentric as well as eccentric loading ($e = -30$ mm).

The presented results reveal a tremendous increase in local vertical strains in the web plate due to discontinuities (i.e. rail joints) in the crane rail. Based on the finite element calculations, the following increase is found: i) concentric wheel loading in Fig. 11a, $\varepsilon_{z,max} = 0.23$ ‰ for continuous rail, $\varepsilon_{z,max} = 0.60$ ‰ for orthogonal rail joint (increase factor 2.61); ii) eccentric wheel loading in Fig. 11c, $\varepsilon_{z,max} = 0.49$ ‰ for continuous rail, $\varepsilon_{z,max} = 0.97$ ‰ for orthogonal rail joint (increase factor 1.98). The corresponding increase in strains for bevel joint is only marginally smaller. The measurement results in Fig. 11b and d show a very similar trend. Considering the measured strains for the cases with continuous rail, it is found that the maximum measured compressive strain is not at the load introduction at x = 0, but at strain gauge position x = –250 mm. The minimum compression strains are found at x = +100 mm. The reason for this 'inverted' distribution mainly lies in the fact that a small gap (<1 mm) between crane rail and top flange was recorded in the region of the load introduction. The finite element results do not consider any unintended gap between the rail and the top flange. Therefore, the numerical results can be interpreted as reference case without any gap. A detailed numerical parametric study investigating the effect of different gap geometries can be found in [9].

Table 1
Investigated parameters of the FE parametric study.

	h_w [mm]	t_w [mm]	b_f [mm]	t_f [mm]	a [mm]	rail type
M0 (test girder)	1900	18	550	30	2200	A120
M1	2000	15	400	20	2000	A100
M2	2000	15	400	40	2000	A100
M3	1000	15	400	20	2000	A100
M4	1000	15	400	40	2000	A100
M5	2000	15	400	20	2000	A55

5. FE parametric study

5.1. Investigated parameters

The results of the previous chapters have shown that the local strains in the web of the test girder are significantly increased in the regions near rail joints. To further generalise and quantify this finding, an additional numerical parametric study was carried out and is presented in this section. The finite element model was based on the model of the test girder in Section 4.1. The geometry parameters were varied as listed in Table 1. The investigated parameters are web height h_w and web thickness t_w, flange width b_f and flange thickness t_f (identical dimensions for both flanges for models M1 to M5, flanges of the test girder in model M0 as in Fig. 4), distance of transverse stiffeners a and rail type. In total six geometry sets were considered.

Model M0 corresponds to the test girder, models M1 and M2 comprise girders with a depth of approximately 2 m with a crane rail of type A100. The flange thickness is 20 mm for model M1 and 40 mm for model M2. Models M3 and M4 generally correspond to models M1 and M2, respectively. However, the depth of the girder is only approximately 1 m. Finally, model M5 comprises a girder of approximately 2 m depth and a rather small crane rail of type A55. For all models M0–M5, in total 16 different loading and contact situations with and without rail joints were investigated. Calculations were done for elastomeric bearing pad as well as for steel bearing plate under the crane rail. For cases with continuous rails and rails with orthogonal joint, eccentric loading with $e = +k/4$ (with k being the width of the rail head in mm) was considered. For cases with bevel rail joint, eccentric loading with $e = \pm k/4$ was considered. Furthermore, the models were calculated with and without rail clips. Thus, 2 contact types · 4 load cases · 2 rail clip configurations = 16 cases for each model, resulting in 96 different basis configurations.

Additional 24 calculations with concentric wheel loading were carried out for models M0 and M1. The results of these 120 numerical simulations (32 with continuous rail, 32 with orthogonal rail joint and 56 with bevel rail joint) are the basis for the investigation of the increase of local strains/stresses in the web due to rail joints.

5.2. Increase factors for maximum vertical stresses due to rail joints

Fig. 12 presents the determined increase factors of maximum local vertical stresses in the web plate due to rail joints. The increase factors were calculated as in the previous section. Fig. 12a shows the results for model M1 based on the maximum vertical strains, Fig. 12b illustrates the results for model M1 based on the maximum vertical stresses. For the test girder in model M0, the vertical strains are determined 40 mm from the top flange, while for models M1-M5, the vertical stresses are taken at a distance of 20 mm from the top flange. In both cases disturbances from the web to flange connection should be avoided. Models M1-M5 were modelled without additional fillet welds, while the test girder (model M0) was modelled with additional fillet welds. Therefore, the distance was larger for model M0. The two increase factors 2.61 and 1.98 that were calculated for the test girder in Section 4.2 (see Fig. 11a,c) for orthogonal rail joint on elastomeric bearing pad are highlighted in Fig. 12a.

The results in Fig. 12 are divided into four curves: orthogonal rail joint and bevel rail joint on elastomeric bearing pad (two solid lines) and orthogonal rail joint and bevel rail joint on steel bearing plate (two dashed lines). The data points left of the vertical dashed lines show the results for concentric wheel loading, while the data points right of these lines show the results for eccentric wheel loading. The latter consist of results in the mid-plane of the web plate and of results on the compression side of the web. A comparison of results for the pure compression cases and the results in the mid-plane of the web due to eccentric loading reveals very similar behaviour. Only the curve for bevel rail joint on elastomeric bearing pad and model M1 in Fig. 12b shows slightly different behaviour. This can be explained by the non-symmetric behaviour of rails with bevel joint, even for cases with concentric loading.

The experimental tests were carried out on the test girder without any rail clips. To investigate the influence of rail clips on the increase factor of local stresses and strains, the parametric study was carried out with and without rail clips. For that purpose, four pairs of rail clips were added to the models M0–M5. The rail clips were positioned over the

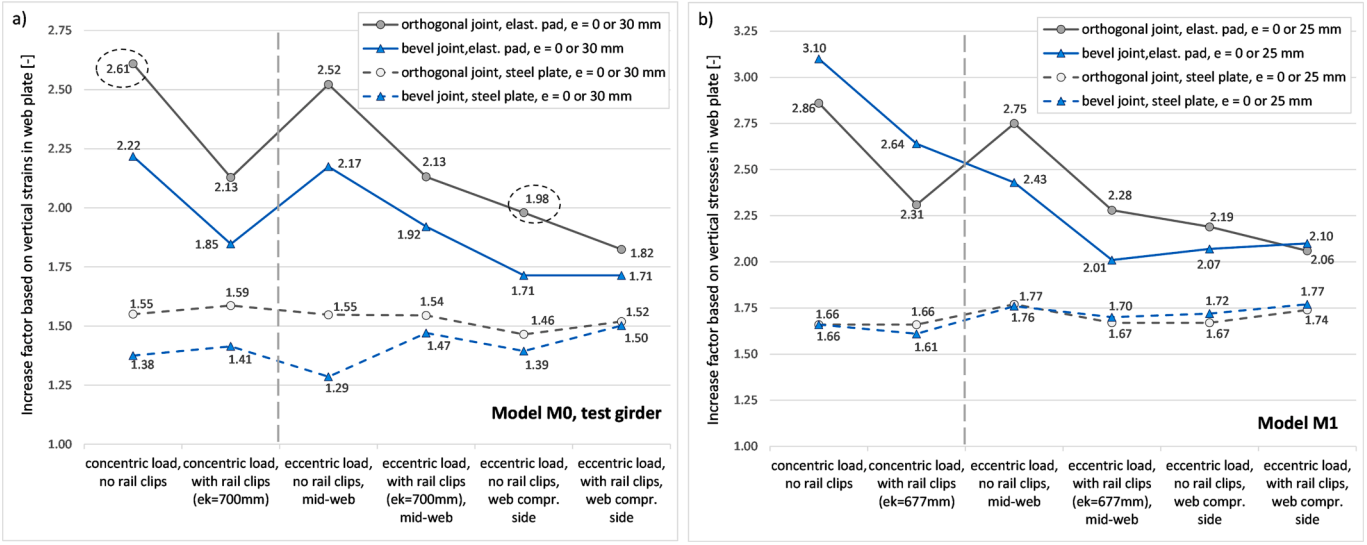

Fig. 12. Increase factor of maximum local vertical strains and stresses in web plate due to rail joints: a) model M0 based on vertical strains, b) model M1 based on vertical stresses.

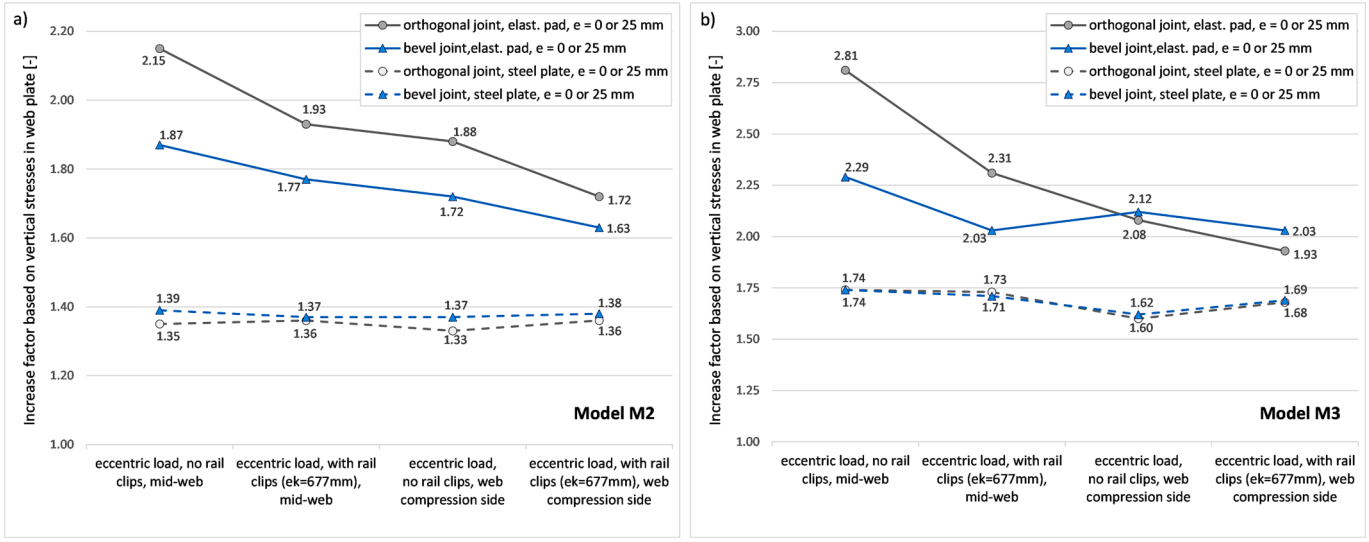

Fig. 13. Increase factor of maximum local vertical stresses in web plate due to rail joints: a) model M2, b) model M3.

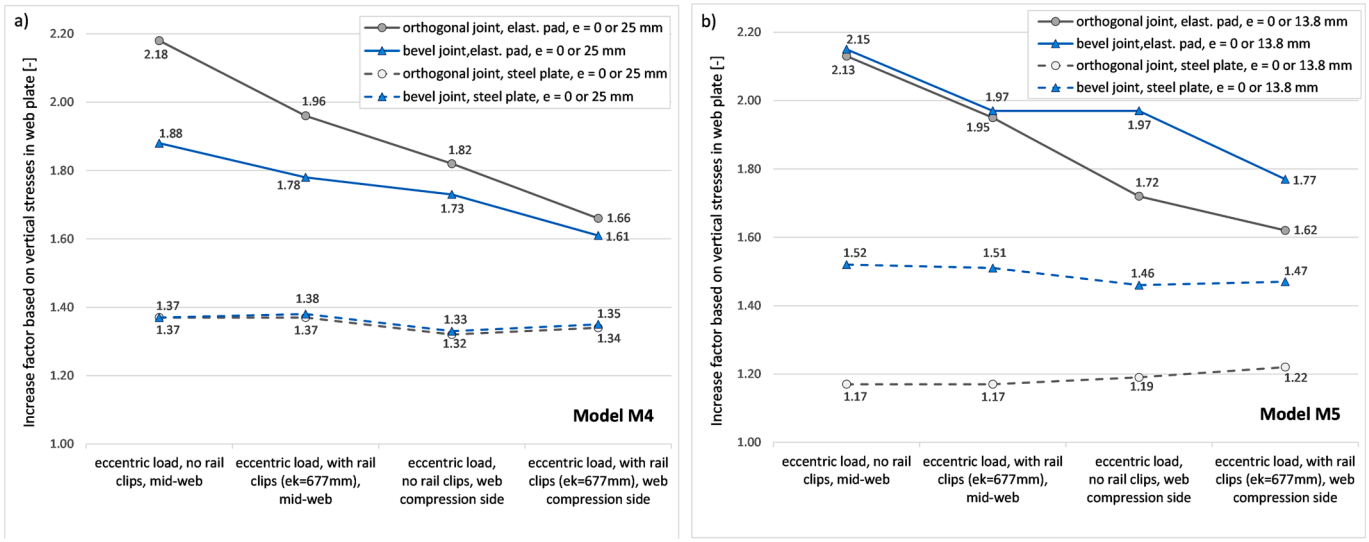

Fig. 14. Increase factor of maximum local vertical stresses in web plate due to rail joints: a) model M4, b) model M5.

transverse stiffeners at the supports and in the third points over the length of the girder. A gap of 1 mm was assumed between the top surface of the rail foot and the contact area of the rail clips. It can be verified from Fig. 12 that the influence of rail clips is negligible for the results with steel bearing plate, but it is significant for the cases with elastomeric bearing pad. This holds true for concentric as well as eccentric wheel loading. This finding can be explained by the fact that the elastomeric bearing pad allows for larger vertical deformations than the steel bearing plate. Therefore, contact between rail foot and rail clip is established earlier for cases with elastomeric rail pad. This leads to smaller stresses in the web directly under the wheel load due to additional global bending in the rail, in particular for cases with rail joints.

Figs. 13 and 14 summarise the increase factors for models M2-M5 in the same way as in Fig. 12. The only difference being that no cases with pure concentric wheel loading were investigated. The presented increase factors of vertical stresses in the web plate for models M0-M5 in Figs. 12–14 reveal the following key results: i) orthogonal rail joints and bevel rail joints show similar increase factors, ii) cases with elastomeric bearing pads show significantly larger increase factors than cases with steel bearing plates (Note: this is due to the loss of the beneficial load distribution effect of the elastomeric bearing plate which is generally present only for continuous rails), iii) the presence of rail clips has hardly any influence on the increase factors for cases with steel bearing plates, while significant influence is found for cases with elastomeric bearing pads (stresses with rail clips are generally smaller, in particular for cases with rail joints), iv) an increase of flange thickness leads to a decrease of the increase factor. This can be verified by comparing the results of model M1 ($t_f = 20$ mm) with model M2 ($t_f = 40$ mm) and the results of model M3 ($t_f = 20$ mm) with model M4 ($t_f = 40$ mm).

Table 2
Summary of stress increase factors due to orthogonal rail joints based on parametric study.

Orthogonal joint	min	mean	max	COV
Concentric[1)], steel plate	1.17	1.52	1.77	0.038
Eccentric, steel plate	1.19	1.45	1.74	0.035
Concentric[1)], elastomeric pad	1.93	2.31	2.86	0.094
Eccentric, elastomeric pad	1.62	1.87	2.19	0.032

1) Including results for concentric loading and results in the mid-plane of the web for eccentric loading.

Table 3
Summary of stress increase factors due to bevel rail joints based on parametric study.

Bevel joint	min	mean	max	COV
Concentric[1)], steel plate	1.29	1.52	1.76	0.025
Eccentric, steel plate	1.33	1.50	1.77	0.024
Concentric[1)], elastomeric pad	1.77	2.13	3.10	0.126
Eccentric, elastomeric pad	1.61	1.85	2.12	0.037

1) Including results for concentric loading and results in the mid-plane of the web for eccentric loading

Tables 2 and 3 give a summary of the stress increase factors due to orthogonal rail joints and bevel rail joints, respectively. Basic statistical results (minimum value, mean value, maximum value and coefficient of variation) are presented for four sub-groups: concentric or eccentric loading with steel bearing plate or elastomeric bearing plate, respectively. The cases with concentric wheel loading effects consist of cases with pure concentric wheel load (only for models M0 and M1) and of cases with eccentric wheel load and consideration of stresses in the mid-plane of the web plate only.

It is found that the maximum increase factors for maximum local vertical stresses for the investigated cases with steel bearing plate range between 1.74 and 1.77 with very low scatter, independent of the eccentricity of the wheel load. Therefore, a slightly conservative approximation of 1.8 is recommended in these cases for practical design purposes. Compared to that, the stress increase factors for cases with elastomeric bearing pad are significantly higher. The minimum stress increase factors for these cases range between 1.61 for eccentric loading and 1.77 for concentric loading. The maximum stress increase factors for elastomeric bearing pads and eccentric wheel load show values of 2.12 for bevel rail joints and 2.19 for orthogonal rail joints. These values increase to 3.10 and 2.86 for concentric loading. The maximum stress increase value of 3.10 for bevel joint type and concentric loading is based on stresses on the compression side of the web (not at mid-plane). This effect is due to the asymmetric nature of this type of rail joint. Taking all results of the conducted parametric study into account, a stress increase factor of 3.1 is suggested for cases with elastomeric bearing pads and concentric loading. A reduced value of 2.2 is recommended for eccentric wheel loads.

5.3. Selected detailed results to show the main effects

Finally, some selected results are summarised in more detail to present the main effects due to rail joints. Further results of the parametric study can be found in [27]. Fig. 15 presents a comparison of local vertical stresses in the web for model M1 (rail type A100) and model M5 (rail type A55), with the same girder type. The continuous rails without joints are concentrically loaded with $F_z = 500$ kN. The stresses in the mid-plane of the web are plotted along the length of the girder at a distance of 20 mm from the top edge of the web. Fig. 15a and c show the results for steel bearing plate without and with rail clips, respectively. Fig. 15b and d present the corresponding results for the cases with elastomeric bearing pad.

The following conclusion can be drawn from the results with concentric wheel loads: i) The presence of rail clips is negligible for concentric wheel loading. The results in Fig. 15a and c are nearly identical. Only minor differences between Fig. 15b and d can be found; ii) The larger crane rail of type A100 for model M1 leads to significantly smaller vertical stresses compared to model M5 with the smaller rail of type A55; iii) The vertical stresses are considerably smaller for cases with elastomeric bearing pad compared to the corresponding cases with

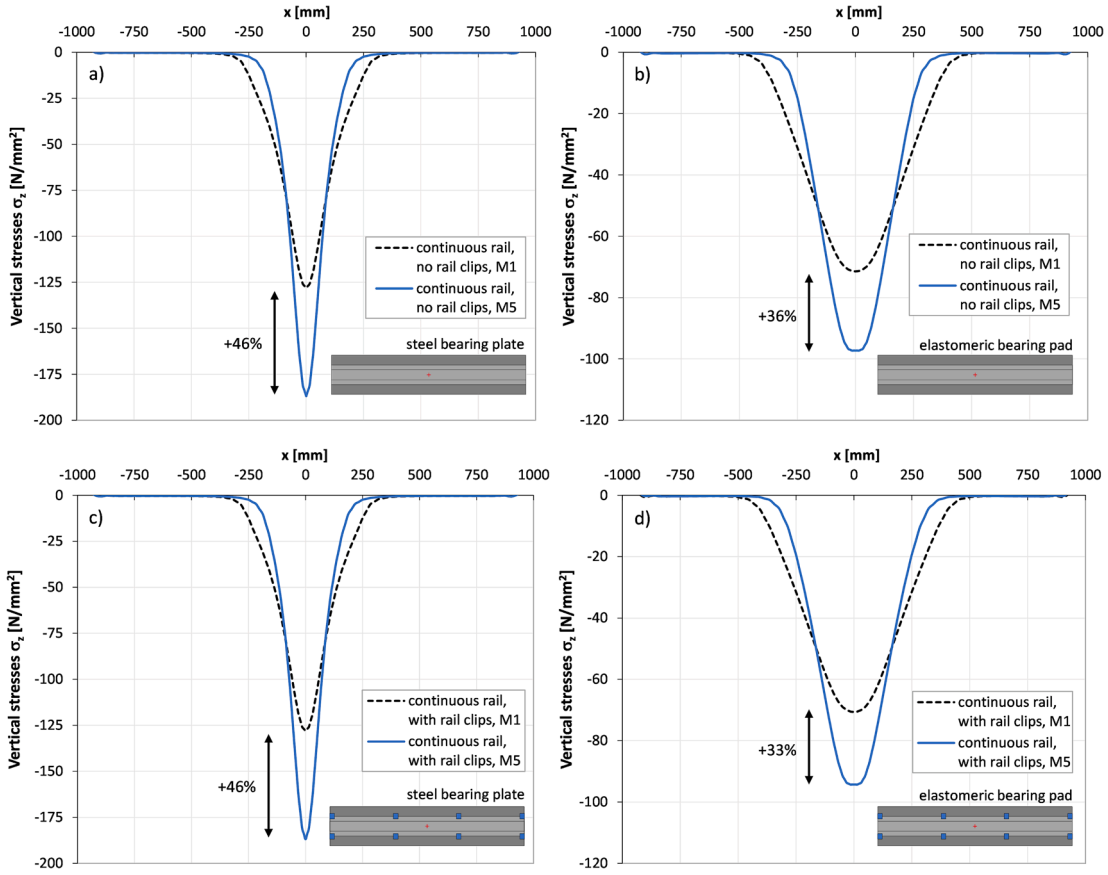

Fig. 15. Comparison of local vertical stresses in the web for model M1 (rail type A100) and model M5 (rail type A55) with continuous rail, $F_z = 500$ kN, $e = 0$: a) no rail clips and steel bearing plate, b) no rail clips and elastomeric bearing pad, c) with rail clips and steel bearing plate, d) with rail clips and elastomeric bearing pad.

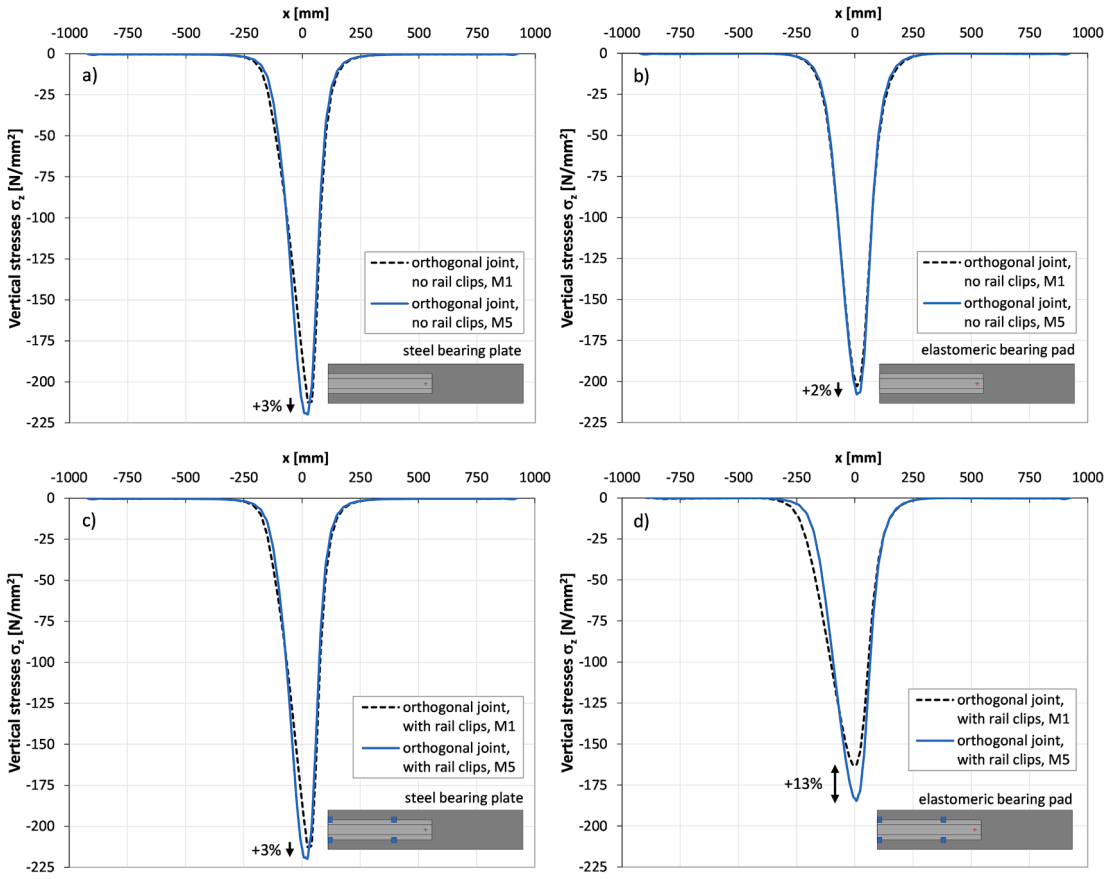

Fig. 16. Comparison of local vertical stresses in the web for model M1 (rail type A100) and model M5 (rail type A55) with orthogonal rail joint, $F_z = 500$ kN, $e = 0$: a) no rail clips and steel bearing plate, b) no rail clips and elastomeric bearing pad, c) with rail clips and steel bearing plate, d) with rail clips and elastomeric bearing pad.

steel bearing plate; iv) The increase of maximum compression stresses from model M1 to model M5 is more pronounced for the cases with steel bearing plate (+46%) than for cases with elastomeric bearing pad (only 33% to 36%).

Fig. 16 presents basically the same comparison of results for the models M1 and M5. The difference to Fig. 15 is that the rail is no longer continuous but shows an orthogonal joint at mid-span, but again with concentric wheel loads.

The comparison of maximum compression stresses for the cases with orthogonal rail joints in Fig. 16 with the corresponding results in Fig. 15 for cases with continuous rails provides eight of the stress increase factors that were presented in Section 5.2 (Fig. 12 for model M1 and Fig. 14 for model M5). Moreover, the following conclusions can be drawn from the results in Fig. 16 for concentric wheel loading: i) The influence of rail size is much smaller for cases with orthogonal joint compared to the reference cases with continuous rails. The maximum vertical compression stresses for model M5 (rail type A55) are only about 3% larger than the stresses for model M1 (rail type A100). Only for the case of elastomeric bearing pad plus rail clips (Fig. 16d), the increase in stresses is about 13%; ii) The presence of rail clips is negligible for concentric wheel loading on rails with orthogonal joint and steel bearing plate. A beneficial influence of rail clips is found for cases with elastomeric bearing pad; iii) The differences in stresses between cases with steel bearing plate compared to cases with elastomeric bearing pad are significantly smaller than for the corresponding cases with continuous rails in Fig. 15.

6. Conclusions

The presented research results confirmed that the maximum local vertical stresses in the webs of crane runway girders are strongly affected by discontinuities of the crane rails. Based on experimental tests as well as numerical parametric studies, stress increase factors for the maximum vertical stresses were developed that characterize the significant increase of local maximum stresses in the region beneath rail joints compared to the reference cases with continuous rails. Orthogonal and bevel rail joints were investigated on elastomeric bearing pad as well as on steel bearing plate. The following main conclusions could be drawn:

- The investigated cases with steel bearing plate revealed maximum stress increase factors ranging between 1.74 and 1.77, independent of wheel load eccentricity. Therefore, a slightly conservative approximation of 1.8 is recommended for practical design purposes.
- The stress increase factors for cases with elastomeric bearing pad were significantly higher. Taking all results of the conducted parametric study into account, a maximum stress increase factor of 3.1 is suggested for cases with concentric loading. A smaller value of 2.2 is recommended for cases with eccentric wheel loads on rails with elastomeric bearing pads.
- The results of the parametric studies for continuous crane rails of types A100 and A55 confirmed that the local vertical stresses in the web are significantly smaller for cases with the larger crane rail of type A100. However, this beneficial influence of rail size vanishes for cases with rail joints.
- By comparing the numerical results of cases with elastomeric bearing pad and with steel bearing plate, it was found that in case of rail joints the maximum vertical strains are approximately of the same size for both cases. This fact was found for concentric as well as for eccentric loading. The typical

beneficial effect of elastomeric bearing pad under the continuous rail was lost due to the orthogonal or bevel rail joint.

Based on the findings that maximum local vertical stresses in the webs at rail joints increase by the factor 2.0 or 3.0 (steel bearing plate or elastomeric bearing pad), it seems advisable to install new crane rails with foot flange without any expansion joints. The connection between the web and the top flange of the crane runway girder anyway represents one of the most decisive criteria for the fatigue design check of welded girders. However, particular care should be taken to ensure that the rail clips allow for free movement of the crane rail in longitudinal direction of the crane runway girder to avoid significant higher longitudinal stresses in the rail.

Declaration of Competing Interest

The authors declare that they have no known competing financial interests or personal relationships that could have appeared to influence the work reported in this paper.

Acknowledgements

The authors would like to thank Assoc.Prof. Bernhard Freytag and his team from the Laboratory for Structural Engineering at Graz University of Technology for the good cooperation and support dealing with the girder tests.

References

[1] Girkmann K. Flächentragwerke. 1st ed. Vienna: Springer; 1945.
[2] Parkes EW. The stress distribution near a loading point in a uniform flanged beam. Philos Trans Royal Soc A 1952;244:417–67.
[3] Rieve JJ. Stabilität I-förmiger Querschnitte unter der örtlichen Lasteinleitung. Bautechnik-Archiv 1953;7:3–31.
[4] Vögele H-G. Ermittlung der Spannungen im Steg von I-Trägern im Lasteinleitungsbereich bei Lastangriff an den Gurten. Der Stahlbau 1972;41:225–31.
[5] Oxfort J. Zur Beanspruchung der Obergurte vollwandiger Kranbahnträger durch Torsionsmomente und durch Querkraftbiegung unter dem örtlichen Radlastangriff. Der Stahlbau 1963;32:360–7.
[6] Oxfort J. Zur Biegebeanspruchung des Stegblechanschlusses infolge exzentrischer Radlasten auf dem Obergurt von Kranbahnträgern. Der Stahlbau 1981;50:215–7.
[7] Kettler M, Derler C, Schörghofer A, Macho C, Unterweger H. Laboratory and numerical tests on real crane runway girder with box section. J Constr Steel Res 2019;160:540–58. https://doi.org/10.1016/j.jcsr.2019.06.002.
[8] Kettler M, Unterweger H, Ebner D. Lokale Spannungen in Kranbahnträgern mit Längssteifen: Experimentelle und numerische Untersuchungen. Stahlbau 2021;90:248–61. https://doi.org/10.1002/stab.202000069.
[9] Kettler M, Unterweger H. Influence of longitudinal stiffeners on the local stresses in crane runway girders - experimental and numerical investigations. Ce/Papers 2022;5:598–605. https://doi.org/10.1002/CEPA.1796.
[10] Steinhardt O, Schulz U. Zur örtlichen Stegbeanspruchung zentrisch belasteter Kranbahnträger bei Verwendung elastisch gebetteter Kranschienen. Der Bauingenieur 1969;44:293–6.
[11] Hoffmann K. Zentrische Lasteinleitung in den Obergurt bei elastisch gebetteten Breitfußschienen - Teil I. Fördern Und Heben 1982;32:36–42.
[12] Hoffmann K. Zentrische Lasteinleitung in den Obergurt bei elastisch gebetteten Breitfußschienen - Teil II. Fördern Und Heben 1982;32:83–7.
[13] Hoffmann K. Auswirkungen der exzentrischen Radlasteinleitung bei elastisch gebetteten Breitfußschienen. Fördern Und Heben 1982;32:898–904.
[14] Kettler M, Kampleitner A, Novak F, Mandl A, Unterweger H. Local stresses in webs of crane runway girders: Tests and numerical calculations. J Constr Steel Res 2017;139:188–201. https://doi.org/10.1016/j.jcsr.2017.09.016.
[15] Kettler M, Zauchner P, Unterweger H. Determination of wheel loads from runway cranes based on rail strain measurement. Eng Struct 2020;213:110546. https://doi.org/10.1016/j.engstruct.2020.110546.
[16] Kettler M, Kiem F, Unterweger H. Local stresses in retrofitted crane runway girders with boxed upper flange due to eccentric wheel loading. Structures 2020;25:646–59. https://doi.org/10.1016/j.istruc.2020.03.024.
[17] Kuhlmann U, Euler M. Beitrag zur Ermüdungsfestigkeit von Schienenschweißnähten bei Kranbahnen. Stahlbau 2009;78:170–9. https://doi.org/10.1002/stab.200910016.
[18] Kuhlmann U, Euler M, Weihe S, Herter KH, Rettenmeier P. Test-based fatigue strength of constructional details with wheel load application - Investigations on partial penetration flange-to-web connections. Stahlbau 2015;84:655–66. https://doi.org/10.1002/stab.201510312.
[19] Euler M, Kuhlmann U. Aufgeschweißte Flach- und Vierkantschienen von Kranbahnträgern: Ermüdungsnachweis für Schweißnähte zur Schienenbefestigung. Stahlbau 2018;87:1101–20. https://doi.org/10.1002/stab.201800016.
[20] Wardenier J, de Vries P, Timmerman G. Fatigue behaviour of a welded I-section under a line load in compression. J Constr Steel Res 2017;128:210–8. https://doi.org/10.1016/j.jcsr.2016.08.022.
[21] Wardenier J, de Vries P, Timmerman G. Fatigue behaviour of a welded I-section under a concentrated compression (wheel) load. J Constr Steel Res 2018;140:163–73. https://doi.org/10.1016/j.jcsr.2017.10.027.
[22] Feldmann M, Citarelli S. Radlastinduzierte Ermüdung bei Kranbahnträgern schwerer Hüttenkrane. Stahlbau 2018;87:1187–98. https://doi.org/10.1002/stab.201800030.
[23] Dürr A, Winkler M. Anwendung von höherfrequenten Hämmerverfahren bei Kranbahnträgern. Stahlbau 2021;90:21–35. https://doi.org/10.1002/stab.202100075.
[24] Seeßelberg C. Typische Fehler bei Planung, Fertigung und Betrieb von Kranbahnträgern und ihre Vermeidung. Stahlbau 2021;90:2–13. https://doi.org/10.1002/stab.202100061.
[25] Rykaluk K, Marcinczak K, Rowiński S. Fatigue hazards in welded plate crane runway girders – Locations, causes and calculations. Arch Civil Mech Eng 2018;18:69–82. https://doi.org/10.1016/j.acme.2017.05.003.
[26] EN 1993-6, Eurocode 3: Design of Steel Structures - Part 6: Crane Supporting Structures, CEN, Brussels, 2009.
[27] Jurschitsch T. Einfluss von Schienenstößen auf die lokalen Spannungen in Stegen von Kranbahnträgern. Master Thesis. Graz University of Technology; 2021.